Research Article Vol. 30, No. 5 / 28 Feb 2022 / Optics Express 6755
Optics EXPRESS

Optimization of pulse self-compression in hollow capillary fibers using decreasing pressure gradients

MARINA FERNÁNDEZ GALÁN,* ENRIQUE CONEJERO JARQUE, AND JULIO SAN ROMAN

Grupo de Investigación en Aplicaciones del Láser y Fotónica, Departamento de Física Aplicada, Universidad de Salamanca, E- 37008, Salamanca, Spain
marinafergal@usal.es

Abstract: The improvement of techniques for the generation of near-infrared (NIR) few-cycle pulses is paving the way for new scenarios in time-resolved spectroscopy and the generation of ultrashort extreme-ultraviolet pulses through high-harmonic generation. In this work, we numerically study how to optimize the self-compression of NIR pulses using decreasing pressure gradients in hollow capillary fibers (HCFs). We identify a moderate nonlinear regime in which sub-cycle pulses are obtained with very good temporal quality from an input 30 fs pulse centered at a 800 nm wavelength and coupled as the fundamental mode of an argon-filled HCF fully evacuated at the output end. Surprisingly, we observe that there is a relatively broad region of parameters for which the optimum self-compression takes place, defined by a simple relation between the input pulse energy and the initial gas pressure.

1. Introduction

High-quality near-infrared few-cycle pulses have become essential tools in disciplines such as ultrafast spectroscopy [1] and attosecond science [2], as they allow to probe the most fundamental properties of matter on extremely short time scales. At present, the most common method for generating intense few-cycle pulses is post-compression in hollow capillary fibers (HCFs), which was proposed and experimentally demonstrated by Nisoli *et al*. in 1996 [3]. These fibers are attractive because of their high damage threshold, which allows for a larger energy scaling than in conventional optical fibers, and the possibility of tuning the nonlinearity and dispersion by changing the filling gas or its pressure [4]. The standard HCF post-compression is based on the nonlinear spectral broadening of an input femtosecond pulse by self-phase modulation (SPM), followed by phase compensation in an external compressor made up of elements such as chirped mirrors, prisms or gratings [5]. In this type of post-compression setups, the input pulse energy is limited due to the appearance of higher-order nonlinear effects such as ionization and self-focusing, which degrade the spectral phase and complicate the subsequent compression [6,7]. To overcome these problems, Nurhuda *et al*. theoretically suggested the use of increasing pressure gradients in the HCF, allowing for a further increase in the pulse energy [8,9]. This method was successfully applied by Suda *et al*. in 2005 to generate sub-10-fs pulses at 800 nm with energies in the mJ level [10]. The continuous advances in this increasing pressure technique, together with the development of the stretched flexible HCFs technology, have led to the generation of high-quality few-cycle pulses with terawatt peak powers [11,12] and the setup has also been extended to different spectral regions [13].

Although HCF post-compression experiments have been greatly optimized, the pulse duration achievable with this method is limited by uncompensated higher-order dispersion and by the difficulty to find efficient compressors in a very broad spectral region. Therefore, to obtain shorter pulses different approaches become necessary. To date, the shorter infrared and visible

#451264 https://doi.org/10.1364/OE.451264
Journal © 2022 Received 14 Dec 2021; revised 29 Jan 2022; accepted 6 Feb 2022; published 15 Feb 2022

Optics EXPRESS

pulses actually measured were created using a light-field synthesizer [14]. Nonetheless, soliton self-compression based on the nonlinear propagation in HCFs, which is one of the most used techniques to generate ultrashort pulses, also offers a promising solution [15–17]. Soliton self-compression relies on the interplay between the negative group-velocity dispersion (GVD) and SPM when the pulse propagates in a region of anomalous dispersion of the fiber. Since this interplay can be very complex and dynamic, it is important to identify the optimal experimental parameters for high-quality self-compression. HCF self-compression experiments have been successfully designed to generate extremely short pulses in different configurations. In particular, soliton self-compression down to the sub-cycle regime has been demonstrated in HCFs filled with gases at constant pressure using pre-compressed pulses [16] and with more standard input pulse durations [17]. Similar results have also been theoretically predicted in microstructured HCFs filled with constant pressure [18]. Moreover, several scaling rules have been recently presented for the case of hollow-core photonic crystal fibers (HC-PCFs) filled with gas at constant pressure [19]. Like in post-compression setups, the use of increasing pressure gradients has also demonstrated to work well for adiabatic soliton compression, but this process requires very long fibers [20]. The use of decreasing pressure gradients in soliton self-compression has been also demonstrated in kagomé HC-PCFs [21,22], and with pre-compressed pulses in HCFs [23], to eliminate the distortions introduced by the transmission through the output windows and deliver the pulses directly to vacuum experiments. It has also been demonstrated that applying a negative pressure gradient can minimize the nonlinear mode coupling and improve the purity of the output beam in the compression of higher-order spatial modes in gas-filled HCFs [24], taking advantage of their greater anomalous dispersion [25].

In this work, we theoretically demonstrate that the use of decreasing pressure gradients can benefit the self-compression of standard near-infrared pulses in the fundamental mode of argon-filled HCFs with typical core sizes by shifting the optimal parameter region towards low energies, thus avoiding the onset of detrimental nonlinear effects such as ionization. Using this technique, we obtain shorter output pulses, with higher peak powers and a better temporal structure when compared to those obtained in the equivalent constant pressure situations. Furthermore, we identify the optimal input parameters for obtaining high-quality sub-cycle pulses showing that there is a relative broad region, defined by a simple relation between the input pulse energy and the average gas pressure, where optimum self-compression can be achieved. These extraordinary laser pulses could be directly delivered to subsequent ultrafast spectroscopy experiments.

2. Numerical model and simulations

To study the nonlinear propagation of a laser pulse through a hollow capillary fiber (HCF), we have numerically solved the one-dimensional generalized nonlinear Schrödinger equation (GNLSE) for the electric-field envelope $A(z,T)$ including the linear losses of the fiber, all the dispersion terms, self-phase modulation (SPM) and self-steepening. In the frequency domain, this propagation equation can be written as [26]:

$$\begin{aligned}\frac{\partial \tilde{A}}{\partial z} + \frac{\alpha(z,\omega)}{2}\tilde{A} - i\left[\beta(z,\omega) - \beta^{(0)}(z) - \beta^{(1)}(z)(\omega-\omega_0)\right]\tilde{A} = \\ = \mathcal{F}\left[i\gamma(z)\left(|A|^2 A + \frac{i}{\omega_0}\frac{\partial}{\partial T}(|A|^2 A)\right)\right],\end{aligned} \tag{1}$$

where $\mathcal{F}$ stands for direct Fourier transform, $\tilde{A}(z,\omega) = \mathcal{F}[A(z,T)]$, z represents the position along the fiber, T is the time measured in a reference frame travelling with the pulse at the group velocity $v_g(z) = 1/\beta^{(1)}(z)$, $\alpha(z,\omega)$ is the absorption coefficient of the HCF, $\beta(z,\omega)$ is the propagation constant, $\beta^{(0)}(z) = \beta(z,\omega_0)$, and $\gamma(z)$ is the nonlinear parameter defined as $\gamma(z) = n_2(z)\omega_0/(cA_{\text{eff}})$, n_2 being the nonlinear refractive index of the filling gas, ω_0 the central frequency, c the speed of

Optics EXPRESS

light in vacuum and A_{eff} the effective modal area, as defined in [26]. Note that the propagation constant, the nonlinear parameter and the fiber losses depend on the propagation coordinate when dealing with pressure gradients.

This 1D equation is good enough to describe the propagation dynamics in a low-intensity regime [8], where the transverse dynamics are negligible, and can be solved with fast integration procedures. In order to validate this model, we have also compared the results of several simulations with a complete 2D propagation model including both the temporal and spatial pulse dynamics, and we have found a perfect agreement between both of them (see Section 3.2). A detailed description of the 2D numerical model, which includes diffraction, dispersion, linear losses, SPM, self-steepening, ionization, losses due to the ionization process and plasma absorption, can be found in [6].

To solve Eq. (1) we have implemented the efficient fourth-order Runge-Kutta in the interaction picture (RK4IP) algorithm [27] in combination with the local error method (LEM) for continuously adapting the step size [28]. The complete linear response is solved in the frequency domain using the analytical expressions for the propagation constant and the absorption coefficient of the EH_{mn} hybrid mode of a hollow dielectric capillary, which are given by [29]:

$$\beta_{mn}(\omega,p) = \frac{\omega}{c} n_{mn}(\omega,p) = \frac{\omega}{c}\left(n_{\text{gas}}(\omega,p) - \frac{u_{mn}^2 c^2}{2\omega^2 a^2}\right), \tag{2}$$

$$\alpha_{mn}(\omega,p) = \left(\frac{u_{mn}}{n_{\text{gas}}(\omega,p)}\right)^2 \frac{c^2}{\omega^2 a^3} \frac{\nu^2(\omega,p)+1}{\sqrt{\nu^2(\omega,p)-1}} \quad ; \quad \nu(\omega,p) = \frac{n_{\text{clad}}(\omega)}{n_{\text{gas}}(\omega,p)}, \tag{3}$$

where p represents the pressure of the filling gas, u_{mn} is the n-th zero of the Bessel function of the first kind $J_{m-1}(x)$, a is the core radius, n_{clad} is the refractive index of the dielectric cladding

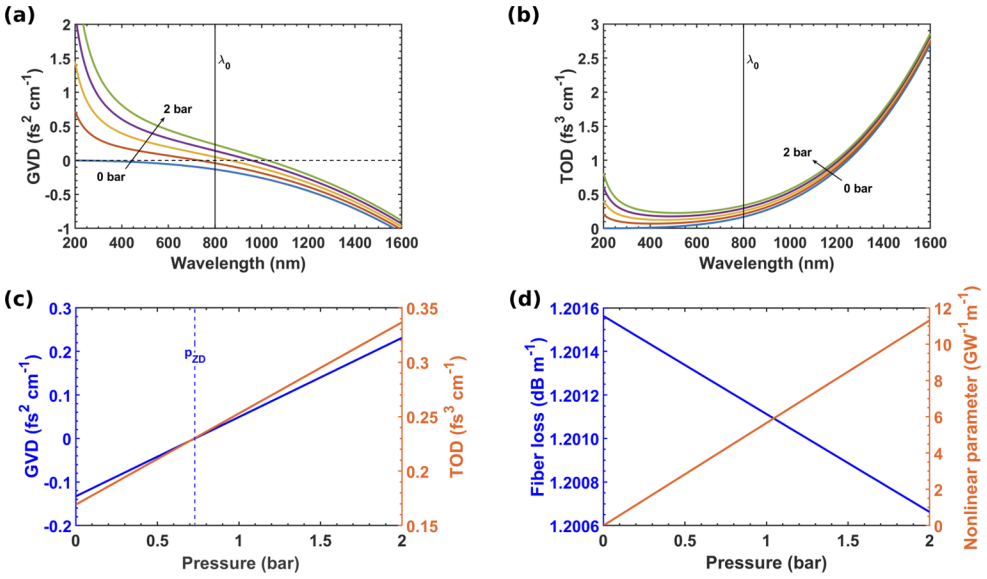

Fig. 1. Dependence of the different parameters appearing in the GNLSE on the pressure of the filling gas. (a) GVD and (b) TOD curves for the fundamental EH_{11} mode of a 100 μm core radius hollow capillary filled with 0 to 2 bar of argon (0.5 bar steps). The vertical solid line indicates the central wavelength at 800 nm. (c) GVD (blue) and TOD (orange) at 800 nm plotted as a function of gas pressure. The vertical dashed line represents the zero-dispersion pressure (730 mbar). (d) Absorption coefficient α (blue) and nonlinear parameter γ (orange) of the EH_{11} mode of the same fiber, both at a central wavelength of 800 nm.

Optics EXPRESS

and n_{gas} is the pressure dependent refractive index of the gas. In our case, we have modeled a fused-silica HCF filled with argon by using the Sellmeier expansion given in [26] for the glass and in [30] for the gas.

Varying the gas pressure affects dispersion, the strength of the nonlinearity and, to a much lesser extent, the linear losses of the fiber. As an example, Fig. 1 shows these parameters for the fundamental EH_{11} mode of a 100 μm core radius fused silica HCF filled with argon. All the dispersion coefficients and the nonlinear parameter scale linearly with the gas density and therefore with pressure. However, the fiber losses decrease very slowly with gas pressure (Fig. 1(d)) due to a minimal increment in the refractive index of the gaseous core as the pressure varies from 0 to 2 bar. Especially important are the two first dispersion coefficients, responsible for group-velocity dispersion $\left(\mathrm{GVD} = (d^2\beta/d\omega^2)_{\omega_0}\right)$ and third-order dispersion $\left(\mathrm{TOD} = (d^3\beta/d\omega^3)_{\omega_0}\right)$, which are plotted as a function of the central wavelength for different argon pressures in Figs. 1(a) and 1(b), respectively. Figure 1(c) shows the dependence of these two coefficients on gas pressure for a central wavelength of 800 nm. As we can see, TOD is always positive and takes its minimum value for $p = 0$, while GVD becomes zero at a pressure p_{zd} known as the zero-dispersion pressure and can take both positive and negative values. For the parameters considered here $p_{zd} = 730$ mbar. When $p<p_{zd}$ the negative waveguide contribution dominates and the dispersion is anomalous, and when $p>p_{zd}$ the dispersion is normal. Finally, for calculating the nonlinear parameter γ shown in Fig. 1(b) we considered $n_2 = 1.08 \times 10^{-19} p\,(\mathrm{cm}^2/\mathrm{W})$ for argon as given in [31], p being the gas pressure measured in bar.

3. Results and discussion

Using the numerical model described in the previous section, we have simulated the nonlinear propagation of a 30 fs (full width at half-maximum, FWHM) transform-limited gaussian pulse at 800 nm in the fundamental EH_{11} mode of a 3 m long, 100 μm core radius fused silica hollow capillary filled with argon. These pulse and fiber parameters are usual in self-compression experiments from commercial systems. In our work, we decided to keep these parameters fixed to limit the number of free variables to a 2D space (gas pressure and input pulse energy) where an optimum region for self-compression could be easily identified. In this space, the optimization is expected to occur at some points which ensure that the fixed fiber length is in between the characteristic self-compression and soliton fission lengths, so as to reach the maximum compression without entering the soliton fission regime, being always in a region of low soliton order ($N<15$) to achieve a high-quality compression [4]. Once the initial pulse duration, central frequency, filling gas and fiber length where chosen, we plotted in the energy-pressure plane the curves where our 3 m propagation distance matched an average compression length for different HCF inner radius. This average length was calculated in terms of the self-compression and fission lengths, using the definitions given in [4,32] (see Supplement 1 for further details). A core size of 100 μm was finally chosen to ensure that the optimization could take place in a region of low pressures, to achieve a strong anomalous response, and moderate input pulse energies, avoiding the appearance of undesirable nonlinear effects such as ionization or self-focusing which were not included in the 1D numerical model. Such a small core HCF offers a good balance between acceptable losses and strong anomalous response.

In the simulations, the input pulse energy has been varied from 50 to 110 μJ and the gas pressure between 100 mbar and 600 mbar, always below the zero-dispersion pressure (730 mbar) to observe soliton self-compression due to the interplay between SPM and the negative GVD. These parameter ranges were enough to include the global optimum for the variable pressure case, as will be shown later on. For higher energies, the complete 2D model demonstrated that ionization and self-focusing could no longer be ignored. For all the points of this region, where the 1D model worked well, we have analyzed both the case when the filling gas is kept at a constant pressure and when a decreasing pressure gradient is applied. The latter can be achieved

Optics EXPRESS

by setting a different pressure value on each fiber end. In this way, if L represents the fiber length and p_0 and p_L are the input and output pressures, respectively, then the pressure distribution along the longitudinal coordinate z of the fiber is given by [10]:

$$p(z) = \sqrt{p_0^2 + \frac{z}{L}\left(p_L^2 - p_0^2\right)}. \tag{4}$$

In order to compare the results obtained with both decreasing and constant pressure, we have matched the integrated nonlinear phase shift acquired by the pulse peak during its propagation, which is also known as the B-integral, as done in similar studies [8,9]. Neglecting the fiber losses, this can be estimated from the expression [23]:

$$B = \int_0^L \gamma(z)P(z)\,dz \approx \tilde{\gamma}P_0 \int_0^L p(z)\,dz = \tilde{\gamma}P_0 \frac{2L(p_0^3 - p_L^3)}{3(p_0^2 - p_L^2)}, \tag{5}$$

where P_0 is the input peak power and $\gamma(z)$ is the nonlinear parameter, that we have expressed in terms of the gas pressure as $\gamma(z) = \tilde{\gamma}p(z)$, $\tilde{\gamma}$ being the value of the nonlinear parameter at a pressure of 1 bar ($\tilde{\gamma} = 5.67 \times 10^{-9}$ W^{-1}m^{-1}bar^{-1} for the parameters considered here). In conventional HCF post-compression setups, where the fiber dispersion is often very weak and the nonlinearity dominates, a similar spectral broadening can be expected from the constant and decreasing pressure situations if the value of the estimated B-integral is the same in both cases. In analogy with this, although even very weak dispersion may be critically important in soliton dynamics, we will use this same criterion to determine which constant and decreasing pressure situations can be said to be equivalent, as done in other studies [23,24]. Focusing on those cases where the output end of the fiber is kept evacuated ($p_L = 0$), one can find that a system with a decreasing gradient is comparable to that with a constant pressure p_{eq} simply if $p_0 = 3p_{\mathrm{eq}}/2$ [23,24]. To arrive to this expression, $P(z)$ in Eq. (5) was assumed to be constant, but if the fiber losses were included, the factor of $3/2$ should actually be slightly different. However, even though the fiber losses can be relatively large in our case, we have found in the simulations that this simple relation surprisingly constitutes an accurate way to compare the different situations, observing quite similar propagation dynamics. We have attributed this to the fact that, during the self-compression process, the peak power of the pulse increases, compensating for the reduction in the total energy, thus making the correction factor negligible.

3.1. Optimal self-compression parameters

In Fig. 2 we have plotted the value of the estimated B-integral as a function of the input pulse energy (E_0) and the equivalent constant argon pressure for a 30 fs pulse propagating in a 3 m long HCF. As we can see, and as is evident from Eq. (5), for fixed values of pulse duration, L and $\tilde{\gamma}$, the curves of constant B-integral in the energy-pressure plane are hyperbolas $E_0 p_{\mathrm{eq}} = \kappa$, with κ a constant. Two of these curves are represented in solid lines in the graph, together with the B-integral value along them.

To identify the optimal input parameters for high-quality self-compression, we have plotted the FWHM duration of the output pulses as a function of the initial pulse energy and the equivalent argon pressure for the constant (Fig. 3(a)) and decreasing (Fig. 3(b)) pressure cases. To have a better idea of the quality of the compressed pulses in both situations, we have also plotted the peak power of the output pulses normalized to its initial value for the same constant ((Fig. 3(c)) and decreasing (Fig. 3(d)) pressure cases. The latter gives us an idea of the temporal structure of the final pulses, which can become very complex due to soliton fission after the point of maximum self-compression. When this happens, the output pulses may sometimes present very short FWHM durations due to the appearance of narrow spikes over a very noisy background. Although apparently very short, these extremely fissioned pulses, which may be useless for many

Optics EXPRESS

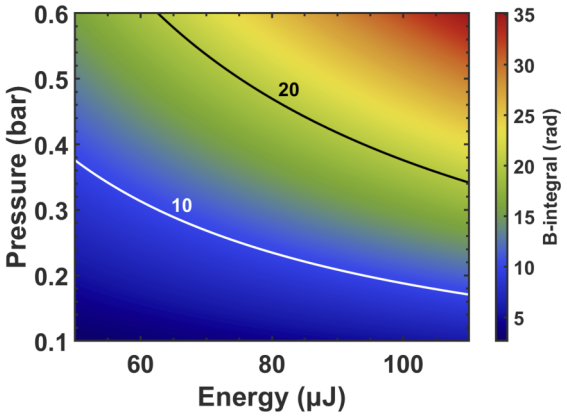

Fig. 2. Map of estimated B-integral as a function of the input pulse energy and pressure for a 30 fs pulse propagating in a 3 m long hollow capillary fiber filled with argon. The pressure on the vertical axis refers to a constant pressure which can be that of a homogeneously filled HCF or the equivalent pressure p_{eq} of a differentially pumped fiber as explained in the text. The solid lines represent two hyperbolas of constant B-integral and the labels next to them indicate their values in rad.

applications, present low peak powers as the total energy is mainly distributed in the surrounding structure. Therefore, in our study we have considered that the output pulses present a good quality when they have both a short FWHM duration and a high peak power at the same time, meaning that they have a clean temporal profile with a main central peak and little secondary structure. Even though it is not the point of our study, it is important to note that this soliton fission process is not always detrimental, but is also the basis of resonant dispersive wave emission, as already demonstrated in several experiments [16,22,23].

In view of the graphs in Fig. 3, it is clear that, for the whole pressure and energy ranges considered here, the self-compression process is substantially enhanced when a decreasing pressure gradient is applied to the filling gas compared to the equivalent constant pressure situations. This result is in accordance with the recently observed behavior in the self-compression of higher-order modes of a HCF [24]. In their study, Wan and Chang already demonstrated an improvement in the self-compression of the higher-order mode which propagated close to its zero dispersion for a given pressure when a decreasing gradient was used. In our case, we have endeavored to work with the fundamental EH_{11} mode of the fiber, which is the most commonly employed mode in experiments, with the difficulty that it presents a very narrow region of anomalous dispersion for near-infrared wavelengths and for typical fiber sizes. Therefore, to observe the desired soliton self-compression, the propagation occurs necessarily close to the zero-dispersion pressure. This increases the importance of higher-order dispersion, which is especially strong near the fiber end where the pulse spectrum is broader. The strong perturbations introduced by higher-order dispersion in the last stages of pulse self-compression can cause the pulse to break, considerably limiting the compression performance. However, with the decreasing pressure gradient, the value of TOD is reduced near the output end of the fiber at the same time as the negative GVD is increased in magnitude, which also contributes to mitigate the effect of higher-order dispersion, allowing for a much better compression, as previously discussed in [24].

Another striking feature of Fig. 3 is that there is not just a single pair of input energy and pressure values that allow for a good compression, but there are several regions of input parameters that can lead to a similar final situation. The optimal parameter regions are distributed in the energy-pressure plane following a periodic pattern around the hyperbolas of constant B-integral. The best final pulses are obtained for B-integral values between 7 and 10 rad, and the situation

Optics EXPRESS

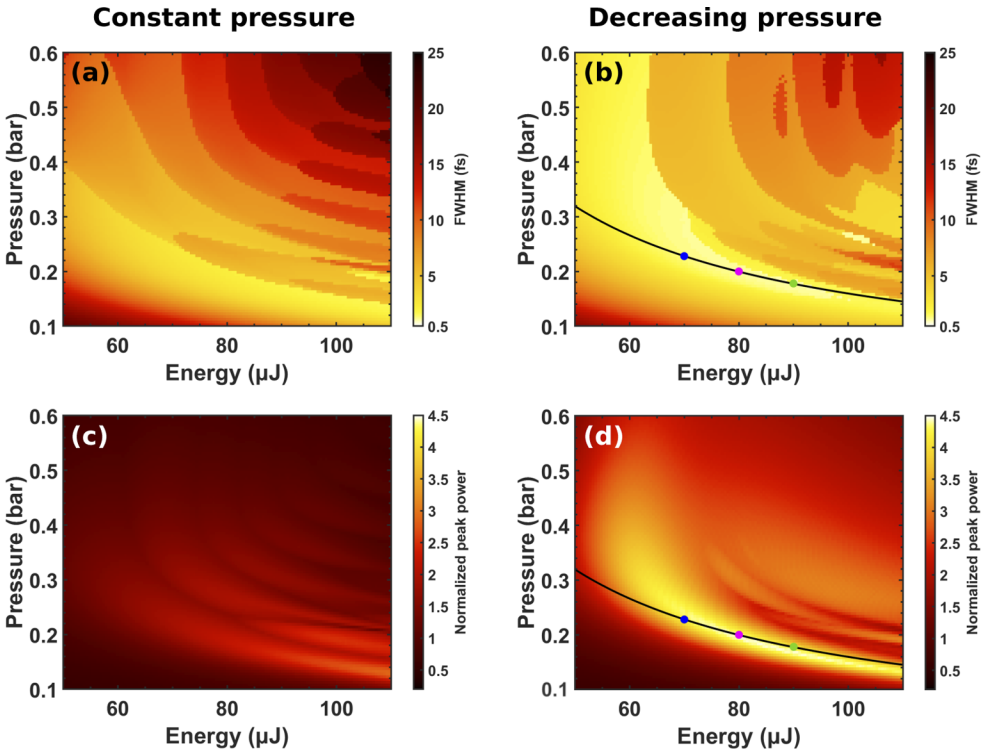

Fig. 3. FWHM duration (top row) of the output self-compressed pulses as a function of input energy and pressure for (a) a statically filled HCF and (b) its equivalent differentially pumped fiber with a decreasing pressure gradient. Peak power of the output pulses normalized to its initial value in each case (bottom row) plotted against the input energy and the equivalent gas pressure for (c) the constant and (d) decreasing pressure situations. The solid black lines in (b) and (d) represent one hyperbola of constant B-integral with a value of $B = 8.5$ rad and the points on it refer to the three situations shown in Fig. 4 with the same colors.

begins to deteriorate as this value increases or decreases. We attribute this to the fact that, for these specific values of accumulated nonlinear phase shift, the compression length approaches the fiber length (see Supplement 1 for more details). When the B-integral is below 7 rad, the pulse experiences a weaker nonlinear interaction and self-compresses slowly. Thus, it would require a longer fiber to reach shorter output durations and higher peak powers. On the other hand, when the B-integral is above 10 rad, the nonlinearity is stronger and the pulse quickly self-compresses, reaching its minimum duration before the fiber output. After that point, it breaks into multiple peaks due to the perturbations introduced by higher-order dispersion. This causes the pulse to stretch as it propagates towards the fiber output, correspondingly reducing the peak power. With the decreasing pressure gradient, the region for optimal self-compression extends further than in the constant pressure case, and there is plenty of room to achieve high-quality, single-cycle or even sub-cycle output pulses. Moreover, taking into account Eq. (5), we have obtained the following simple and useful relation between the optimum initial pressure p_0^{opt} and the input peak power P_0:

$$p_0^{\text{opt}} = \frac{12.75}{\tilde{\gamma} P_0 L}, \tag{6}$$

where we have used $B^{\text{opt}} = 8.5$ rad as the optimum value for the estimated B-integral. This value can be determined by looking for a point in the energy-pressure plane where the fiber length

Optics EXPRESS

is in between the self-compression and the soliton fission lengths. For the fiber, pulse and gas parameters used here, we found that this region can be approximately delimited by estimated B-integral values between 7 and 10 rad, 8.5 rad being the average optimum value (see Supplement 1 for more details). When varying other parameters such as the input pulse duration, central wavelength, fiber length or core radius, similar optimal regions can be systematically found at other input energies and gas pressures, as also shown in Supplement 1.

From Figs. 3(a) and 3(c) it seems that, in the constant pressure case, the self-compression begins to improve towards the lower right corner of the grid, i.e. lower pressure and higher energy. We have not extended the parameter scans further towards this region because the 1D model could be inaccurate due to an increasing importance of ionization and self-focusing in argon. These effects could be ameliorated by using harder gases such as helium, as has already been done to experimentally self-compress NIR pulses to durations of around 1 fs in HCFs with constant gas pressure [16]. However, when working with gases with low ionization potentials, such as argon, the decreasing pressure technique would be especially useful as it helps to alleviate these detrimental nonlinear effects by shifting the optimal self-compression region towards lower energies.

In Fig. 3 we can also note that, with both constant and decreasing pressure, the optimal region for self-compression becomes narrower towards the lower corner of the graphs. Therefore, in the case of constant gas pressure, the optimization would take place in a very narrow region, that would fall along the same hyperbola with $B = 8.5$ rad, around 250-280 μJ and 40-50 mbar according to the approximated simulations performed with the 1D propagation model. However, we have verified with the 2D model that the propagation of the pulse in this energy and pressure region differs from that obtained with the 1D model due to the presence of ionization in argon. Therefore, the global optimum would still be the one shown in Fig. 3 for the decreasing pressure gradient. Moreover, such a small region in the parameter space would complicate the experimental setup as slight deviations from the optimal input parameters would generate strongly fissioned output pulses, making them useless for many purposes. Hence, another strength of the decreasing pressure technique is that it allows to achieve optimal self-compression in a wider range of input energies and gas pressures as compared to the constant pressure case. Furthermore, it allows to deliver the self-compressed pulses directly to vacuum experiments, limiting the perturbations introduced by the transmission windows and the gas cell, as already suggested elsewhere [21–24].

Figure 4 shows the self-compressed pulses obtained at the fiber output in three different situations with the same value of B-integral of 8.5 rad, corresponding to the cases marked with colored points at the region of optimal compression in Fig. 3. From left to right, the input energy was 70, 80 and 90 μJ, and the equivalent constant pressure, 228, 200 and 178 mbar, respectively. The pulses plotted in colored lines were obtained when a decreasing pressure gradient was applied to the filling gas in the HCF, and those plotted in grey lines were obtained when the gas was kept at the equivalent constant pressure. As we can see, in this regime the output pulses are much better in the decreasing pressure case as they have shorter durations, higher peak powers and less structure than those obtained with constant pressure. The complex temporal structure appearing in the trailing edge of the pulses is due to the perturbations introduced by higher-order dispersion in the last stages of the self-compression process, which cause the pulse to break, and grows as the input energy increases. This structure is clearly more pronounced in the constant pressure cases, which confirms that the decreasing pressure gradient effectively limits the impact of higher-order dispersion terms. We can also notice that the main peak of the output pulses is less shifted towards the trailing edge when the decreasing pressure gradient is used, which means that the pulses undergo a smaller self-steepening than in the fiber filled with constant pressure, also resulting in a slightly lower pedestal in their leading edges. This can be understood by recalling that with the decreasing pressure gradient, the strength of the nonlinearity is gradually

Optics EXPRESS

reduced as the pulses propagate through the HCF and therefore the impact of self-steepening is also limited at the end of the compression process.

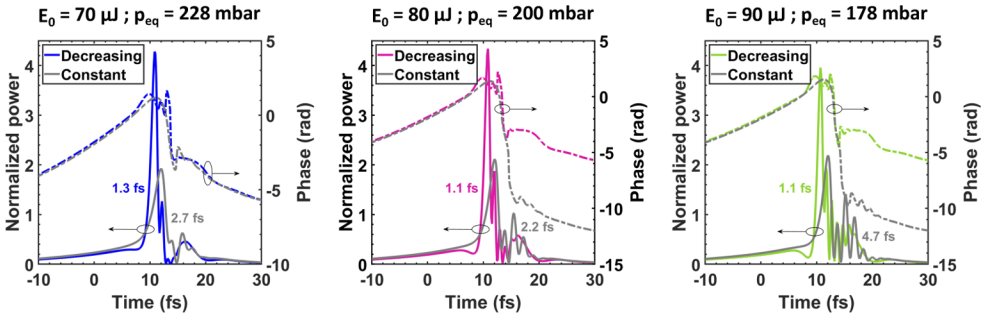

Fig. 4. Self-compressed pulses at the fiber output for three different pairs of values of input energy E_0 and equivalent pressure p_{eq} lying along the same hyperbola of constant B-integral with B = 8.5 rad. The pulses plotted in colored lines were obtained when a decreasing pressure gradient with the square root profile was applied to the filling gas in the fiber, and the grey lines represent the pulses obtained when the gas was kept at the equivalent constant pressure p_{eq} in each case. The three situations correspond to the points shown in Figs. 3(b) and 3(d) with the same color code. The solid lines refer to the power profile (left axis), while the dot-dashed lines represent the temporal phase (right axis). In all the graphs, the power is normalized to the corresponding initial peak power and the labels next to each pulse represent the FWHM durations.

From left to right in Fig. 4, the output pulses obtained from the differentially pumped fiber reached sub-cycle FWHM durations of 1.3, 1.1 and 1.1 fs, and peak powers of 9.4, 10.9 and 11.2 GW, respectively. Such short durations are possible thanks to a large spectral broadening towards high frequencies, which shifts the central wavelength of the pulse peak to shorter wavelengths [17]. In the equivalent constant pressure cases, the FWHM durations of the output pulses were 2.7, 2.2 and 4.7 fs, and the peak powers, 4.2, 5.3 and 6.2 GW, respectively. Furthermore, we have also verified that the self-compressed pulses were closer to their Fourier limit in the decreasing pressure situations than in the constant pressure ones.

We should also note that the decreasing pressure gradient continuously shifts the zero-dispersion frequency (ZDF) towards higher frequencies at the same time as the pulse spectrum broadens by SPM. This clearly benefits the self-compression process as more of the generated frequencies end up propagating with anomalous dispersion than in the constant pressure case, where the value of the ZDF is fixed. To illustrate this, in Fig. 5(a) we have plotted the evolution of the ZDF and the central frequency (calculated at each propagation distance as the first moment of the spectrum) during the propagation of a 30 fs, 70 μJ pulse launched in the EH_{11} mode of a 100 μm core radius, 3 m long argon-filled HCF with both constant and decreasing pressure such that p_{eq} = 228 mbar (same cases as in Fig. 4 left). In addition, Figs. 5(b) and 5(c) show the values of GVD and TOD computed as a function of the propagation distance at the corresponding pressure and central wavelength in both cases. As we can see, when the gas is kept at constant pressure, the central frequency ν_0 is blue-shifted approaching the fixed ZDF. As a result of this blue-shifting, both the negative GVD and the TOD decrease in magnitude, following the trend shown in Figs. 1(a) and 1(b). On the other hand, the decreasing gradient continuously moves the ZDF away from the central frequency, causing the anomalous GVD to increase in magnitude. This, together with a steady reduction of TOD due to both the drop in pressure and the spectral blue-shifting, assists the self-compression and limits the impact of higher-order dispersion, as explained before.

Optics EXPRESS

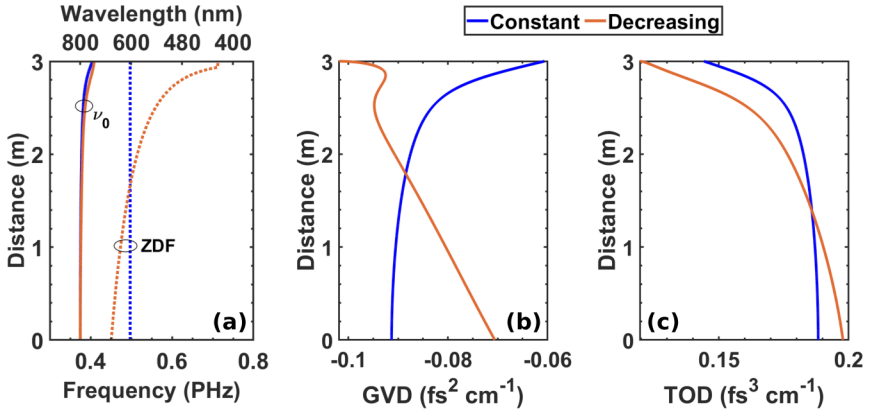

Fig. 5. (a) Evolution of the zero-dispersion frequency ZDF (dotted lines) and the central frequency ν_0 (solid lines) during the propagation of a 30 fs, 70 μJ pulse launched in the EH_{11} mode of a 100 μm core radius, 3 m long argon-filled HCF with both constant (blue) and decreasing (orange) pressure such that p_{eq} = 228 mbar. (b) GVD and (c) TOD as a function of the propagation distance, computed at the corresponding central wavelengths.

3.2. *Comparison with the complete 2D model*

As stated in Section 2, the results shown in Fig. 3 were obtained using a 1D model which allows for a very fast performance of the numerical simulations and, therefore, for the scanning of a wide region of the input parameter space. To investigate the importance of other nonlinear effects such as self-focusing or ionization, and the role of higher-order modes in the pulse propagation dynamics, we have also performed some simulations with a complete 2D model. In our self-compression regime, defined within the parameter region used in Fig. 3, we have found that the results of the 2D model are in perfect agreement with the predictions of the 1D analysis and, therefore, the latter constitutes an efficient fast way to define the optimal regions of the parameter space to achieve high-quality self-compressed pulses when working in a regime of moderate nonlinearity.

As an example, in Fig. 6 we have plotted the results obtained with both numerical models for the propagation of a 70 μJ pulse launched in the fundamental mode of the differentially pumped HCF with a decreasing pressure gradient such that p_{eq} = 228 mbar (same case as in Fig. 4 left). Figures 6(a) and 6(b) show the complete evolution of the normalized power distribution along the fiber obtained with the 1D and 2D models, respectively, and Fig. 6(c) shows a comparison of the output self-compressed pulses in both cases. In a similar way, Figs. 6(d) and 6(e) represent the evolution of the spectrum during propagation obtained with the 1D and 2D models, respectively, and in Fig. 6(f) we have plotted the output spectra in both cases together for comparison. As we can see, all the results obtained with both models are almost identical, which means that in the moderate intensity regime where we are working, processes such as ionization or self-focusing due to nonlinear mode coupling do not play a significant role during the pulse propagation. The main difference that we can notice between the results obtained with both models in Fig. 6 is a slightly greater structure in the high frequencies spectral region of the 2D model, which comes from the emission of dispersive waves in the EH_{12} and EH_{13} modes. However, this does not have an important influence in the overall pulse dynamics.

Optics EXPRESS

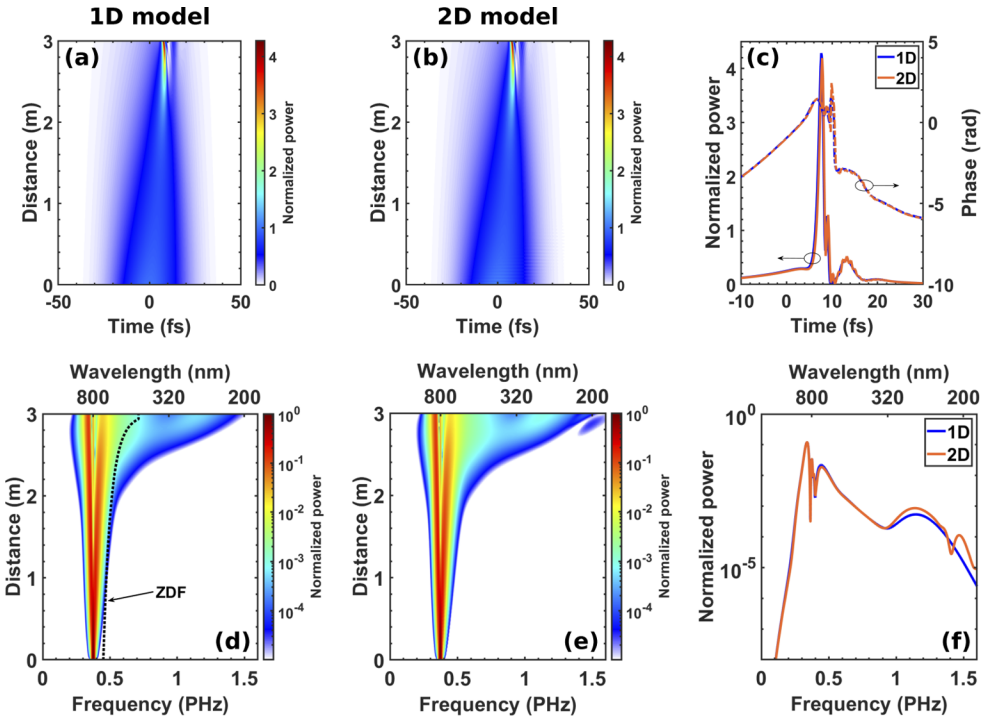

Fig. 6. Comparison of the results obtained with the 1D and 2D numerical models for the propagation of a 30 fs, 70 µJ pulse launched in the EH_{11} mode of a 100 µm core radius, 3 m long HCF filled with argon with a decreasing pressure gradient such that p_{eq} = 228 mbar. The top row shows the evolution of the power distribution along the fiber obtained with the (a) 1D and (b) 2D models, and (c) the output self-compressed pulses in both situations. In a similar way, the bottom row shows the evolution of the spectrum during propagation obtained with the (d) 1D and (e) 2D models, and (f) a comparison of the output spectra in both cases. In all the graphs, both the temporal and spectral power are normalized to their initial peak value. The dotted black line in (d) represents the evolution of the zero-dispersion frequency (ZDF) during propagation through the decreasing pressure gradient.

4. Conclusion

By means of numerical simulations, we have identified the optimum regime to obtain sub-cycle near-infrared (NIR) pulses by soliton self-compression in a single gas-filled hollow capillary fiber (HCF) with a decreasing pressure gradient. In particular, we have systematically studied the nonlinear propagation of an input 30 fs pulse centered at 800 nm in the fundamental mode of a 3 m long differentially pumped argon-filled HCF fully evacuated at the output end, which constitutes a feasible experimental setup. For these parameters, we have identified the optimum input pressure and pulse energy, showing that there is a relatively broad area where high-quality self-compression can be achieved. Furthermore, we have also found a simple relation between the gas pressure and the input pulse energy based on the B-integral, which can be used to define the optimum parameter region. In addition to the intrinsic experimental advantage of decreasing pressure gradients to couple the output pulses directly to vacuum experiments, we have also shown that they can considerably improve the compression when compared to the equivalent constant pressure situation in a regime of moderate pulse energies. Using this variable pressure technique, the last stages of the self-compression process are carried out in a region of low pressure, as far as possible from the zero dispersion, limiting the perturbations introduced

Optics EXPRESS

by higher-order dispersion and nonlinear effects. This allows to generate shorter pulses, with higher peak powers and a cleaner temporal structure as compared with the ones obtained with constant pressure. By comparing the results obtained with our one-dimensional model with a complete bi-dimensional propagation model that also includes all the spatial modes of the fiber, self-focusing and gas ionization, we have verified that the spatial effects are negligible in the moderate-intensity regime where the optimization takes place for the decreasing pressure gradient case. We believe that these findings will pave the way for a new generation of experiments in time-resolved spectroscopy.

Funding. Agencia Estatal de Investigación (PID2019-106910GB-I00).

Acknowledgments. This work was supported by grant PID2019-106910GB-I00, funded by the Spanish Ministry of Science and Innovation, MCIN/AEI/ 10.13039/501100011033.

Disclosures. The authors declare no conflicts of interest.

Data availability. Data underlying the results presented in this paper are not publicly available at this time but may be obtained from the authors upon reasonable request.

Supplemental document. See Supplement 1 for supporting content.

References

1. M. Maiuri, M. Garavelli, and G. Cerullo, "Ultrafast spectroscopy: state of the art and open challenges," J. Am. Chem. Soc. **142**(1), 3–15 (2020).
2. P. B. Corkum and F. Krausz, "Attosecond science," Nat. Phys. **3**(6), 381–387 (2007).
3. M. Nisoli, S. De Silvestri, and O. Svelto, "Generation of high energy 10 fs pulses by a new pulse compression technique," Appl. Phys. Lett. **68**(20), 2793–2795 (1996).
4. J. C. Travers, W. Chang, J. Nold, N. Y. Joly, and P. St. J. Russell, "Ultrafast nonlinear optics in gas-filled hollow-core photonic crystal fibers," J. Opt. Soc. Am. B **28**(12), A11–A26 (2011).
5. T. Nagy, P. Simon, and L. Veisz, "High-energy few-cycle pulses: post-compression techniques," Adv. Phys.: X **6**(1), 1845795 (2021).
6. E. C. Jarque, J. San Roman, F. Silva, R. Romero, W. Holgado, M. A. Gonzalez-Galicia, B. Alonso, I. J. Sola, and H. Crespo, "Universal route to optimal few- to single-cycle pulse generation in hollow-core fiber compressors," Sci. Rep. **8**(1), 2256 (2018).
7. A. Crego, E. C. Jarque, and J. San Roman, "Influence of the spatial confinement on the self-focusing of ultrashort pulses in hollow-core fibers," Sci. Rep. **9**(1), 9546 (2019).
8. M. Nurhuda, A. Suda, K. Midorikawa, M. Hatayama, and K. Nagasaka, "Propagation dynamics of femtosecond laser pulses in a hollow fiber filled with argon: constant pressure versus differential gas pressure," J. Opt. Soc. Am. B **20**(9), 2002–2011 (2003).
9. M. Nurhuda, A. Suda, M. Kaku, and K. Midorikawa, "Optimization of hollow fiber pulse compression using pressure gradients," Appl. Phys. B **89**(2-3), 209–215 (2007).
10. A. Suda, M. Hatayama, K. Nagasaka, and K. Midorikawa, "Generation of sub-10-fs, 5-mJ-optical pulses using a hollow fiber with a pressure gradient," Appl. Phys. Lett. **86**(11), 111116 (2005).
11. F. Böhle, M. Kretschmar, A. Jullien, M. Kovacs, M. Miranda, R. Romero, H. Crespo, U. Morgner, P. Simon, R. Lopez-Martens, and T. Nagy, "Compression of CEP-stable multi-mJ laser pulses down to 4 fs in long hollow fibers," Laser Phys. Lett. **11**(9), 095401 (2014).
12. V. Cardin, N. Thiré, S. Beaulieu, V. Wanie, F. Légaré, and B. E. Schmidt, "0.42 TW 2-cycle pulses at 1.8 μm via hollow-core fiber compression," Appl. Phys. Lett. **107**(18), 181101 (2015).
13. Z. Huang, D. Wang, Y. Dai, Y. Li, X. Guo, W. Li, Y. Chen, J. Lu, Z. Liu, R. Zhao, and Y. Leng, "Design of intense 1.5-cylce pulses generation at 3.6 μm through a pressure gradient hollow-core fiber," Opt. Express **24**(9), 9280–9287 (2016).
14. M. Hassan, T. T. Luu, A. Moulet, O. Raskazovskaya, P. Zhokhov, M. Garg, N. Karpowicz, A. Zheltikov, V. Pervak, F. Krausz, and E. Goulielmakis, "Optical attosecond pulses and tracking the nonlinear response of bound electrons," Nature **530**(7588), 66–70 (2016).
15. L. F. Mollenauer, R. H. Stolen, J. P. Gordon, and W. J. Tomlinson, "Extreme picosecond pulse narrowing by means of soliton effect in single-mode optical fibers," Opt. Lett. **8**(5), 289–291 (1983).
16. J. C. Travers, T. F. Grigorova, C. Brahms, and F. Belli, "High-energy pulse self-compression and ultraviolet generation through soliton dynamics in hollow capillary fibres," Nat. Photonics **13**(8), 547–554 (2019).
17. C. Brahms, F. Belli, and J. C. Travers, "Infrared attosecond field transients and UV to IR few-femtosecond pulses generated by high-energy soliton self-compression," Phys. Rev. Res. **2**(4), 043037 (2020).
18. A. Ermolov, K. F. Mak, M. H. Frosz, J. C. Travers, and P. St. J. Russell, "Supercontinuum generation in the vacuum ultraviolet through dispersive-wave and soliton-plasma interaction in a noble-gas-filled hollow-core photonic crystal fiber," Phys. Rev. A **92**(3), 033821 (2015).

Optics EXPRESS

19. D. Schade, F. Köttig, J. R. Koehler, M. H. Frosz, P. St. J. Russell, and F. Tani, "Scaling rules for high quality soliton self-compression in hollow-core fibers," Opt. Express **29**(12), 19147–19158 (2021).
20. R. Chen, Z. Shi, and G. Chang, "Pre-chirp-managed adiabatic soliton compression in pressure-gradient hollow-core fibers," Photonics **8**(9), 357 (2021).
21. K. F. Mak, J. C. Travers, N. Y. Joly, A. Abdolvand, and P. St. J. Russell, "Two techniques for temporal pulse compression in gas-filled hollow-core kagomé photonic crystal fiber," Opt. Lett. **38**(18), 3592–3595 (2013).
22. C. Brahms, D. R. Austin, F. Tani, A. S. Johnson, D. Garratt, J. C. Travers, J. W. G. Tisch, P. St. J. Russell, and J. P. Marangos, "Direct characterization of tuneable few-femtosecond dispersive-wave pulses in the deep UV," Opt. Lett. **44**(4), 731–734 (2019).
23. C. Brahms, F. Belli, and J. C. Travers, "Resonant dispersive wave emission in hollow capillary fibers filled with pressure gradients," Opt. Lett. **45**(16), 4456–4459 (2020).
24. Y. Wan and W. Chang, "Effect of decreasing pressure on soliton self-compression in higher-order modes of a gas-filled capillary," Opt. Express **29**(5), 7070–7083 (2021).
25. B. A. López-Zubieta, E. C. Jarque, I. J. Sola, and J. San Roman, "Theoretical analysis of single-cycle self-compression of near infrared pulses using high-spatial modes in capillary fibers," Opt. Express **26**(5), 6345–6350 (2018).
26. G. P. Agrawal, *Nonlinear Fiber Optics* (Academic Press, 2013).
27. J. Hult, "A fourth-order Runge-Kutta in the interaction picture method for simulating supercontinuum generation in optical fibers," J. Lightwave Technol. **25**(12), 3770–3775 (2007).
28. A. M. Heidt, "Efficient adaptive step size method for the simulation of supercontinuum generation in optical fibers," J. Lightwave Technol. **27**(18), 3984–3991 (2009).
29. E. A. J. Marcatili and R. A. Schmeltzer, "Hollow metallic and dielectric waveguides for long distance optical transmission and lasers," Bell Syst. Tech. J. **43**(4), 1783–1809 (1964).
30. A. Börzsönyi, Z. Heiner, M. P. Kalashnikov, A. P. Kovács, and K. Osvay, "Dispersion measurement of inert gases and gas mixtures at 800 nm," Appl. Opt. **47**(27), 4856–4863 (2008).
31. D. Wang, Y. Leng, and Z. Xu, "Measurement of nonlinear refractive index coefficient of inert gases with hollow-core fiber," Appl. Phys. B **111**(3), 447–452 (2013).
32. C. M. Chen and P. L. Kelley, "Nonlinear pulse compression in optical fibers: scaling laws and numerical analysis," J. Opt. Soc. Am. B **19**(9), 1961–1967 (2002).